Marine Biology 95, 275–287 (1987)

Marine Biology
International Journal on Life in Oceans and Coastal Waters

Skeletal calcification patterns in the sea urchin *Tripneustes gratilla elatensis* (Echinoidea: Regularia)

I. Basic patterns

J. Dafni and J. Erez

H. Steinitz Marine Biology Laboratory, The Hebrew University of Jerusalem; Box 469, Eilat 88103, Israel

Abstract

A comprehensive study on skeletal calcification in the regular echinoid *Tripneustes gratilla elatensis* was carried out between 1979 and 1981 in the northern Gulf of Eilat (Red Sea), employing size measurement, allometry and radiotracer techniques. Uptake rates of the isotope ^{45}Ca were used to estimate the calcification rate of whole tests. Calcification rates of the different skeletal parts and the ^{45}Ca uptake along the sutural margins of individual plates were also measured. Whole-test calcification rates for juvenile individuals, 11 to 13 mm in diameter, relative to their skeletal Ca dry weight, calculated using the allometric relationship between skeletal dry weight and diameter, were 1.5 to 1.8% d^{-1} for 4 to 8 h of incubation, while calcification rates obtained from periodical size measurements and allometrical constants amounted to 2.75% d^{-1}. The apparent discrepancy between these results is explained partly by the short duration of the incubations, during which the internal calcium pools, apparently in the coelom, were not fully saturated with the radioactive tracer. This discrepancy decreased when longer radioactive incubations were used, or when a post-incubational deposition of ^{45}Ca from these pools was allowed. The size of these pools is roughly 10 μmol Ca per 13-mm individual, and it resides probably in the coelom where Ca concentration is ~3 times higher than in seawater. The calcification rates given as percentage of skeleton added per day, both for the radioactive and allometric methods, decreased with the urchins' size. The calcification patterns of various components of the skeleton generally fitted their allometrical trends – a relative decrease in the size of the spines, apical plates and lantern. The teeth calcify rapidly to compensate for the constant erosion of their tips. Calcification per plate decreased exponentially from the apex to the peristome. Plate-edge calcification patterns of both interambulacral and ambulacral plates fitted patterns derived from size increment measurements, using natural growth-lines. Typically, most plates grow more horizontally (latitudinally) than vertically. It is suggested that the vertical vs horizontal calcification ratio (v/h) determines the individual plate growth and affects the whole test morphology.

Introduction

Although it is fundamentally an endoskeleton made of calcareous ossicles embedded in mesodermic tissue, the echinoid test functions as an exoskeleton of tight-fitted plates surrounding a fluid-filled cavity, the coelom. The plate consists of a tri-dimensional stereom, apparently of monocrystalline high-magnesium calcite (Raup, 1966), filled with a fluid-like tissue termed stroma. The high mechanical stability of the test (Raup, 1968; Weber *et al.*, 1969; Strathmann, 1981) is derived from a combination of compression-resistant rigid plates and tension-resistant collagen fibers at the sutures (Moss and Meehan, 1967, 1968; Telford, 1985).

Traditionally, growth rates and patterns of sea urchins have been obtained from size measurements of live individuals (Fuji, 1967; Ebert, 1968; Vadas, 1977). Plate-edge growth patterns are derived from growth-line patterns (Deutler, 1926; Märkel, 1975, 1976, 1981; White *et al.*, 1985). The radiotracer method, in which the incorporation of the calcium isotope ^{45}Ca is used to determine calcification in marine organisms (Wilbur and Jodrey, 1955; Goreau, 1959; Barnes and Crossland, 1977, 1982; Böhm, 1978), has been employed in the study of echinoderms by Heatfield (1970) and Kaneko *et al.* (1981 b). However, these studies did not address the relationship between urchin size and skeletal calcification. A recent attempt to compare calcification rates of echinoderms (asteroids) with actual growth (Nauen and Böhm, 1979) has shown very much lower calcification rates. In echinoids, ^{45}Ca assays have demonstrated that certain tissues show much higher calcification rates than expected from their relative Ca concentrations (Kaneko *et al.*, 1981 b, 1982). The purpose

of the present study is to check the applicability of the radioactive technique for detailed experimentation of skeletal growth and morphology and to test hypotheses concerning environmental influences (Dafni, 1980, 1983 b, 1985; Dafni and Erez, 1982).

The pathway of skeletal Ca is through various compartments, by which the ion may be stored or retained for a considerable time (Borowitzka, 1979). This apparently affects its deposition kinetics. Different pathways have been suggested for various marine organisms from time-course experiments (Böhm and Goreau, 1973; Böhm, 1978; Borowitzka, 1979, Kaneko *et al.*, 1981 a, b). The largest fluid-filled cavity in echinoids is the coelom, 29 to 35% of the total wet weight. It has normal Ca concentrations 30% higher than the ambient seawater (Kaneko *et al.*, 1982), taking-up within 1 to 2 d ^{45}Ca radioactivity twice as high as the external. Afterwards the activity of the coelomic fluid decreases with the increase of skeletal radioactivity (Kaneko *et al.*, 1981 b). The rapid turnover of Ca in the coelom suggests that it might be a necessary station in the pathway of skeletogenic Ca.

Although echinoid species differ in their average plate porosity (Weber, 1969; Jensen, 1972), due to the different stereom types (Smith, 1980), no attempt was made to relate plate porosity with differential growth and calcification rates.

This paper documents skeletal calcification rates, obtained from ^{45}Ca incorporation and from skeletal size measurements (=allometrically derived), of the sea urchin *Tripneustes gratilla elatensis* (Dafni, 1983 a), and compares calcification patterns in the various skeletal components with allometric trends. While this paper concentrates on the basic patterns, a companion paper (Dafni and Erez, 1987) deals with calcification patterns of abnormal urchins and reports the results of various experiments.

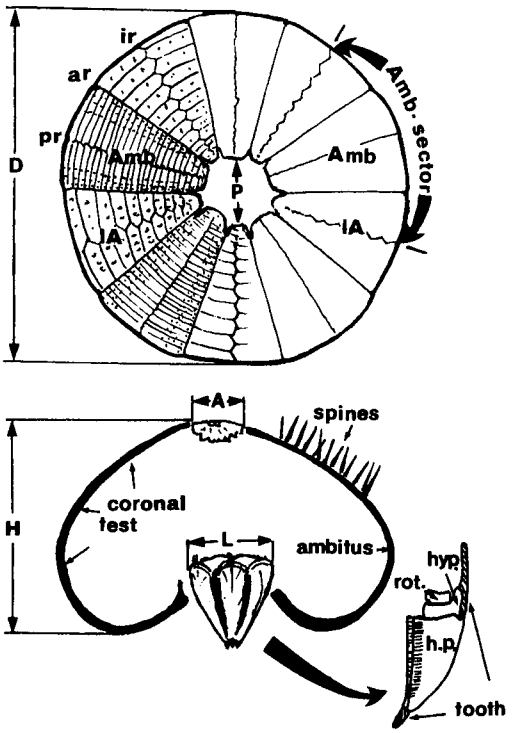

Fig. 1. *Tripneustes gratilla elatensis.* Diagramatic test oral view (top) and cross-section (bottom) showing measureable parameters and analysed components. D: test diameter; H: height; A: apical system diameter; P: peristome width; L: lantern diameter. An ambulacral sector consists of a whole ambulacrum (Amb) and the attached interambulacral (IA) columns. on either side. Meridional sutures that separate the columns are: pr: perradial; ir: interradial; ar: adradial. Lantern sub-units are shown separately – h.p.: half-pyramids (jaws); hyp.: hypophysis; rot: rotula; and tooth, the latter protruding above and below the half-pyramide (proximal and distal ends)

Materials and methods

Morphometric analysis

Live *Tripneustes gratilla elatensis* and denuded tests of different sizes were collected subtidally in the Gulf of Eilat (Red Sea) in 1980, measured and weighed using caliper and a top-loading balance (±0.001 g) in order to obtain the following measurements (Fig. 1): ambital diameter (D); test height (H); apical region diameter (A); peristome diameter (P); Aristotle's lantern width (L); live wet weight (LW) and skeletal dry weight (DW) of bleached (in 5% NaOCl) and oven-dried tests. All the morphometric measurements were correlated through Huxley's (1932) allometry equation:

$$Y = a X^b \quad \text{or} \quad \ln Y = b \ln X + \ln a, \qquad (1)$$

where X and Y are the parameters compared (e.g. diameter, weight etc.), b=allometry coefficient (regression slope of Y vs X), and a="scale ratio", criterion of size order and geometric similarity (Gould, 1966). Comparing equi-dimensional parameters (e.g. length to height, weight vs volume), b=1 is the "exponent of isometry", b > 1 indicates an increase of Y/X with size, whereas b < 1 denotes a relative decrease (positive and negative allometry). When Y represents area or volume and X is mono-dimensional, the exponents of isometry are 2 and 3, respectively.

Following Ricker's (1973) suggestion that, in allometry, where both parameters are interdependent, b/r (r=correlation coefficient) should be preferred as the allometry coefficient, being the average of two regression slopes, i.e. of Y vs X and X vs Y, this measure was adopted here.

Plate porosity was determined from size measurements (plate length, width and thickness – used to calculate their volume, Vp) and from their skeletal dry weight (DW). Since *Tripneustes gratilla elatensis* calcite is composed of 90.25% $CaCO_3$ and 9.75% $MgCO_3$ (Raup, 1966), the specific density (Sd) of the mineral fraction is a weighted average between both components' densities ($Sd = 0.9025 \times 2.710 + 0.0975 \times 2.985 = 2.737$, when 2.710 and 2.985 = specific densities of $CaCO_3$ and $MgCO_3$, respectively). The stereom porosity of a plate is thus defined (Chamberlain, 1978):

$$\%\text{Porosity} = 100 \times [1 - Dw/(Sd \times Vp)]. \qquad (2)$$

^{45}Ca labelling

Time-course experiments. Live *Tripneustes gratilla elatensis* were collected subtidally and pre-incubated for 24 h in transparent 2.5-liter plastic jars at 25 °C ± 1 C° and continuous fluorescent illumination. They were incubated in radioactive seawater (RSW) with a ^{45}Ca radioactivity of 8.3 mCi/mol Ca. Samples of RSW (0.1 ml) were taken and measured in a liquid scintillation counter (Packard, tricarb 3255), after adding 3 ml InstaGel scintillation fluid (Packard) to 5-ml plastic minivials. RSW specific activity (cpm/mg Ca) was determined by dividing counts per minute (cpm) by the Ca content of seawater in the Gulf (0.0482 mg/0.1 ml: Krumgaltz, 1982), and corrected for a counting efficiency of 90%. Since *T. gratilla elatensis* calcite contains 10% $MgCO_3$ (Raup, 1966), a correction was made for a $CaCO_3$/echinoid calcite weight ratio of 0.9 in order to estimate calcification rates in skeletal tissue. Thus, the correction coefficient (C.eff) was $0.9 \times 0.9 = 0.81$.

The urchins treated were divided into three experimental groups: Group 1: 17 individuals of 11 to 14 mm diameter, from which pairs were drawn at various intervals within 24 h; Group 2: three urchins of equal size (13.5mm), maintained in the RSW for 30 d; and Group 3: four individuals (11 to 13.5 mm) which were transferred after 24 h of incubation into non-radioactive seawater (NRSW) for an additional 29 d. All were fed the green alga *Ulva lactuca* (L.). Long-term experiments (> 24 h) were under a 14 h light: 10 h dark regime, constant aeration and controlled temperatures.

Post-incubation processing included piercing of the peristome, evacuation of the coelomic fluid, and four NRSW rinses, followed by distilled water rinse. Later the urchins were sacrificed, bleached in 5% NaOCl for 24 h, rinsed over a GF/F (Whatman) filter, and oven-dried (60 °C). The calcareous material, consisting of the test, spines, Aristotle's lantern etc., was then mortar-crushed and subsamples of 10 to 20 mg, weighted using a Cahn microbalance (± 1 μg), were counted after dissolution in 1 ml H_3PO_4 (0.5 M), in 5-ml plastic scintillation vials, with 2 ml InstaGel.

Two urchins which were dipped for 0.5 min into liquid nitrogen prior to the radioactive assay, and two 5% NaOCl cleaned tests, served as dead controls. Both were exposed to the RSW for 24 h.

Size-dependent calcification rates. Seventeen urchins (11 to 72 mm) were incubated singly for 6 to 8 h in 1 to 3 liters RSW. Afterwards they were processed as above. However, samples for ^{45}Ca counting from urchins < 20 mm included calcareous material from the entire skeleton, whereas in individuals > 20 mm only a fifth of the test, one representative ambulacral (Amb) sector was taken, not including spines and lantern (Fig. 1).

Calcification rates of skeletal parts. Six urchins (20 to 35 mm) were incubated singly for 6 h, and post-incubated for 24 h in NRSW. Radioactive counting was preceded by NaOCl cleaning and weighing in a microbalance of the following skeletal parts (Fig. 1): (1) coronal test, represented by an Amb sector; (2) apical plates; (3) spines and (4), Aristotle's lantern – represented by one jaw and its ossicles. Lantern components were analysed separately: (5) half-pyramids, two of which comprise one jaw; (6) hypophyses; (7) rotulae and (8) teeth. In several individuals, both the upper (proximal) and lower (distal) ends of the teeth were sampled.

Calcification rates of coronal plates. Eight individuals (22 to 72 mm) were incubated for 6 to 8 h in RSW. After cleaning, all interambulacral (IA) plates of a meridional column were separated, weighed and their radioactivity counted.

Sutural growth and differential calcification. Four urchins, with diameters of 34, 49, 54 and 72 mm, were incubated for 6 to 8 h in RSW. Parallel sections, 0.3-mm-wide, were removed from the plate-edges, using a scalpel, from all four sutural edges (Fig. 2A) of each interambulacral plate (IA) of one meridional column. Samples were also taken from the median part of the plate. The samples were processed as above and counted. A somewhat different method was applied to ambulacral plates, because of their smaller size. The perradiad (facing the ambulacral midsuture) triangle and the adradiad margin (bordering the IA plates) were sampled first, and the remaining part cut into adapicad (upper) and adorad (lower) components (Fig. 2B). Because of their large number (> 80), every fifth plate was sampled. In one specimen (49 mm), this procedure was repeated for four columns and the average recorded.

The morphometrically determined accretion rate pattern was obtained from an IA plate column of a 51-mm *Tripneustes gratilla elatensis,* cleaned and charred in a muffle furnace to reveal light and dark growth-line patterns (Pearse and Pearse, 1975) (Fig. 3). Following Deutler (1926), an arbitrary growth-line was selected, from which the distance to the adjacent sutural margin was measured in all four directions (adradiad, interradiad, adapicad and adorad), using an eyepiece micrometer mounted on a dissecting microscope (×40).

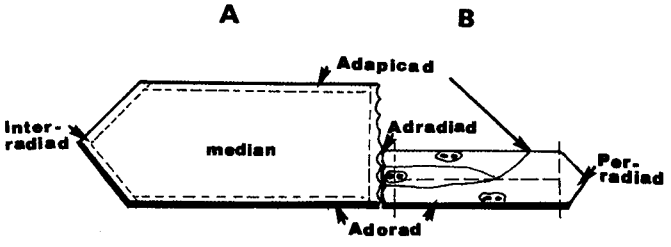

Fig. 2. *Tripneustes gratilla elatensis.* Sampling method for analysis of sutural calcification. A: Interambulacral; and B: Amb plates. Broken lines denote mode of plate-edge removal (for details see text)

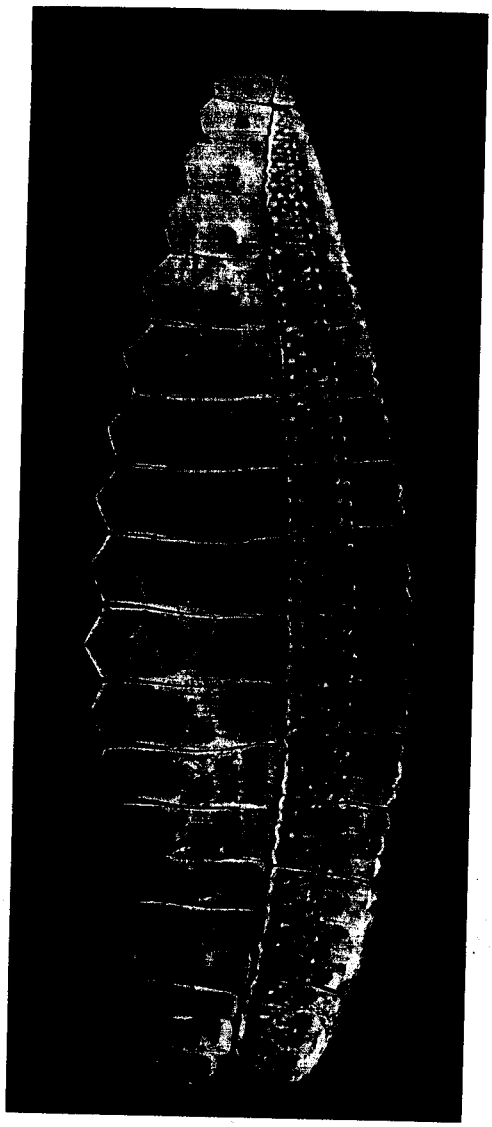

Fig. 3. *Tripneustes gratilla elatensis.* Coronal, IA (left) and Amb plate columns of a medium-sized individual, viewed in transmitted light after charring and embedding in Canada Balsam. Arrows point at growth-lines pattern used for growth measurements

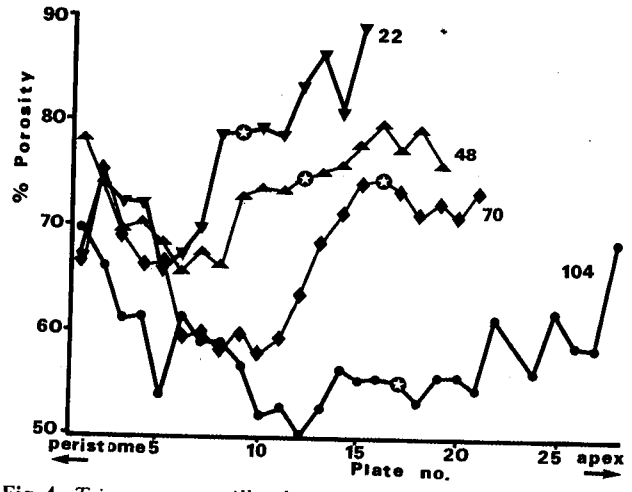

Fig. 4. *Tripneustes gratilla elatensis.* Skeletal porosity of IA plate columns of urchins of various sizes (22 to 104 mm). Asterisks mark the approximate position of the ambitus

Results

Morphometric analysis

The allometrical constants for *Tripneustes gratilla elatensis* are presented in Table 1, where the following trends emerge:

Height vs diameter. The present analysis showed that healthy *Tripneustes gratilla elatensis* have a slightly positive allometry between H and D ($b/r = 1.024$, Table 1 A), so urchins become taller with age.

Relations between apex width and test diameter. A distinctly negative allometry ($b/r = 0.824$, Table 1 B) exists between these parameters, implying slower growth of the apical plate complex, relative to the coronal test.

Aristotle's lantern–peristome relationship. Although both the peristome aperture and lantern diameter are inversely related to the test diameter, the peristome allometry with diameter is more negative (0.803 vs 0.824, Table 1 C, D). This may support the hypothesis (Dafni, 1980) that lantern growth induces peristome expansion. This is also indicated by the positive allometry between lantern and peristome ($b/r = 1.045$, Table 1 E).

Relation between weight and ambital diameter. The allometry coefficients of live wet weight (LW) and skeletal dry weight (DW) vs diameter were 2.980 and 2.796, respectively (Table 1 F, G). LW was almost isometric, whereas the significantly negative allometry between DW and diameter indicates that skeletal weight is relatively decreasing with size. The ratio between DW and LW in a 10-mm *Tripneustes gratilla elatensis* is 0.145, descending to 0.104 at 60 mm. Larger individuals (> 80 mm) tend, however, to grow more slowly, without decreasing their calcification, as reflected by a positive allometry ($b/r = 4.41$) between skeletal weight and diameter (Dafni, unpublished observations).

Porosity. Fig. 4 shows that the porosity of a test plate decreases with the urchin's size and depends on its meridional position relative to the apex. The sereom porosity of super-ambital plates of smaller individuals is $> 80\%$, while in the largest individual measured it decreases to $< 60\%$. Ambital and sub-ambital plates are less porous. Regardless of urchin's size, the plates bordering the peristome are less compact than ambital plates. Since new plates are added continuously, while the plates' position relative to the peristome does not change (because no plates are eliminated adorally: Jensen, 1972; Märkel, 1975), one may suggest that plate porosity decreases with distance from its apical origin, apparently due to $CaCO_3$ deposition within the stereom framework. Slow-growing species, such as *Heterocentrotus mammillatus* (Ebert, 1982), have a more compact stereom ($< 40\%$ porosity) (Weber, 1969; Dafni, unpublished observations). The relatively low

Table 1. *Tripneustes gratilla elatensis.* Calculated allometric relations. a, b = regression constants, and r = correlation coefficient; b/r = allometry coefficient. All size measurements expressed in mm, weight in mg. CI = 95% confidence interval was calculated for b/r. N = number of measured individuals

	Measured parameters		N	Regression constants				95% CI
	X	Y		a	b	r	b/r	
A	Diameter	Height	101	0.501	1.021	0.997	1.024	1.012–1.036
B	Diameter	Apical diameter	36	0.454	0.779	0.946	0.824	0.789–0.858
C	Diameter	Peristome	85	0.757	0.798	0.994	0.803	0.786–0.820
D	Diameter	Lantern	36	0.609	0.806	0.978	0.824	0.785–0.862
E	Peristome	Lantern	36	0.778	1.022	0.978	1.045	1.019–1.071
F	Diameter	Wet weight	79	0.415	2.974	0.998	2.980	2.996–2.995
G	Diameter	Skeletal dry weight	73	0.092	2.771	0.991	2.796	2.732–2.859

Table 2. *Tripneustes gratilla elatensis.* ^{45}Ca determined calcification rates of 11- to 13-mm individuals (means ± SD). –: no data

Duration of exposure	N	μg Ca/mg skeletal $CaCO_3$ *incorporated*		*Net calcification rates*[b]	
		Samples (range)	Control[a]	% h^{-1}	% d^{-1}
Time 0	2	0.006–0.009	–	–	–
0.5 h	2	0.258–0.290	0.109	0.10 ± 0.01	2.44 ± 0.24
1 h	2	0.369–0.460	0.163	0.08 ± 0.01	1.86 ± 0.36
2 h	2	0.505–0.581	0.204	0.05 ± 0.01	1.26 ± 0.13
4 h	2	1.040–1.042	0.217	0.06 ± 0.00	1.52 ± 0.01
8 h	2	1.909–2.407	0.218	0.07 ± 0.01	1.80 ± 0.29
24 h	3	4.450–4.705	0.218	0.05 ± 0.00	1.31 ± 0.08

[a] Subtracted dead control was calculated according to Eq. (3)
[b] Multiplied by molecular weight of $CaCO_3$ (100) divided by atomic weight of Ca, (40) divided by 100, and corrected for an efficiency of 0.81 (see "Time-course experiments" section)

porosity of the plates next to the peristome may result from the precipitation there of a low porosity stereom, in the form of the perignathic girdle (Märkel, 1975).

Calcification rates and patterns

Time-course experiments. The results of the incubation of the first group show that absolute ^{45}Ca incorporation into the skeletons increases with length of exposure (Table 2). The low incorporation of time-0 control (0.008 μg Ca/mg $CaCO_3$) indicates that the post-incubation processing removed all the labelling solution, and contamination during processing was minimal. The incorporation of the skeletal control, 0.049 μg Ca/mg $CaCO_3$ per 24 h, is most probably due to isotopic exchange or adsorption. The relatively higher incorporation of the liquid nitrogen frozen dead control (0.218 μg Ca/mg $CaCO_3$ per 24 h, which is 5% of the live urchins') could possibly be caused by Ca incorporation of the organic tissues and its deposition during processing. Since this control incorporation also includes that of the bare skeleton, the frozen control rates were discounted from the experimental to obtain net calcification values.

Following Borowitzka (1979), who found that dead and decalcified algae exchange Ca with the surrounding seawater exponentially, with a half-time of 0.5 h, the subtracted dead control for the various incubation times was calculated according to the equation:

$$\text{Dead control} = \text{Co}\,[1-\exp(-t \cdot \ln 2/0.5)], \quad (3)$$

when Co = 24 h Ca incorporation of the dead control (0.218 μg/mg $CaCO_3$) and t = exposure in hours. To enable comparison with calcification rates determined in other methods, all calcification rates were expressed as % d^{-1}.

The rates shown in 0.5 h exposure (2.4% d^{-1}) decreased to 1.3% after 2 h, rising to 1.5 to 1.8% d^{-1} in the 4- to 8-h samples. Rates for 24 h were slightly lower (1.3% d^{-1}), possibly due to deterioration of growth conditions in the small experimental jars. The low absolute counts in the first 2 h rendered these samples highly sensitive to calculation mistakes and possible contamination. Therefore we included in our calculations only values obtained from 4 to 8 h. Hence, the average daily calcification rate (Cr) is 1.66 ± 0.20% d^{-1}.

An alternative method to obtain calcification rates was to find the daily growth rate, and calculate the calcification from the allometric relations between cleaned dry

weight (DW) and the urchin's diameter. This, hereafter termed allometric calcification (ADC) rate (Cb) was calculated from the allometry constants (Table 1G) and a growth curve constructed for *Tripneustes gratilla elatensis* field populations, based on Johnson's (1935) equation (Dafni, 1984):

$$St = S_\infty \cdot \exp[-1/k\,(t-t_0)] = 130 \cdot \exp[-1/0.00227\,(t+162)], \quad (4)$$

where St = diameter, t = days after apparent recruitment, and 130 mm is the asymptotic size (S^∞); $k = 0.00227\ d^{-1}$ is the growth constant, and $t_0 = 162$ d. This last constant denotes time elapsed from settlement of metamorphosed post-larvae to the apparent recruitment size (4 mm). Setting t for consecutive days in this equation, the daily size increment was obtained for any initial size. For a 13-mm urchin (mean size of Group 1) $Cb = 3.5\%\ d^{-1}$, and the ratio between the radioactive and allometric rates (F ratio) was:

$$F = Cr/Cb = 1.66/3.5 = 0.47. \quad (5)$$

Long-term experiments. Initially 13.5 mm, the Ca incorporation of the urchins incubated for 30 d in RSW amounted to 0.099 ± 0.017 mg Ca/mg $CaCO_3$ (calculated by dividing the cpm by the final specific activity, allowing for radioactive decay). Their final diameters were 17.2, 18.5 and 18.8 mm. Since there was no direct way to measure dry skeletal weight (DW) of live urchins, and due to partial loss of calcareous material during processing, both initial and final DW (DWi and DWf) were derived indirectly from diameter measurements, using the DW vs D allometry (Table 1G). Calculated DWi and DWf of these urchins were 133.1 ± 23.7 mg and 306.4 ± 39.1 mg, respectively. Hence, the added $CaCO_3$ per individual (C) was:

$$C = 0.099 \times 306.4 \times 2.50/0.81 = 94.11 \pm 6.22 \text{ mg } CaCO_3 \text{ per urchin}, \quad (6)$$

where 2.50 is the ratio between the molecular weights of $CaCO_3$ and Ca and 0.81 is C · eff, a correction coefficient (see Materials and methods). In the long-term incubations, dead controls were ignored. Assuming that calcification rate was uniform throughout this period, the estimated daily ^{45}Ca incorporation rate (Cr, %) is:

$$Cr = \ln[(133.1+94.1)/133.1] \times 100\%/30\ d = 1.79 \pm 0.44\%\ d^{-1}. \quad (7)$$

From the initial and final average sizes (13.5 and 18.2 mm, respectively) and the allometric constants, the allometric calcification rates (Cb), were calculated as $2.76\%\ d^{-1}$. The ratio between the radioactive and allometric rates was:

$$F = 1.79/2.76 = 0.65. \quad (8)$$

The purpose of the following experiment, RSW incubation for 24 h, followed by 29 d of non-radioactive seawater (NRSW) post-incubation, was to show that radioactive Ca, apparently incorporated into the animal tissue during RSW incubation, is deposited later, thus compensating for non-radioactive Ca incorporation during RSW incubation. Cb was measured as above and Cr was estimated from the final skeletal radioactivity, corrected to ^{45}Ca decay. A correction was made for post-incubation of non-labelled Ca, using their DWi/DWf ratios. Hence, for the first 24 h of radioactive exposure, Cr estimate was high, $2.18 \pm 0.61\%\ d^{-1}$, whereas the allometric calcification rate (Cb) was $2.74 \pm 0.52\%\ d^{-1}$, and the F-ratio was 0.79.

The differences between F-ratios of the different experiments are discussed below.

Calcification rate vs size. The size dependence of whole-test calcification rates (CR), for 17 urchins (12 to 72 mm), incubated for 6 to 8 h, is given in Fig. 5. The following equation, fitted by regression, relates calcification rate to diameter (D):

$$Cr = 2.85 \exp(-0.053\ D) \quad (r = 0.949, n = 17) \quad (9a)$$

or logarithmically:

$$\ln Cr = \ln 2.85 - 0.053\ D. \quad (9b)$$

The allometric calcification rates (Cb) were calculated from the growth-curve [Eq. (4)] and allometrically derived DW, and plotted against D:

$$\ln Cb = \ln 6.42 \exp(-0.047\ D) \quad (r = 0.998). \quad (10)$$

Although both curves decline with size (Fig. 5), the former's slope is somewhat steeper (−0.057 vs −0.047). Consequently, the F-ratio between these slopes is also inversely related to size:

$$F = 0.44 \exp(-0.006\ D). \quad (11)$$

The calculated F-ratios for 10- and 60-mm urchins are 0.41 and 0.29, respectively. This subject is addressed in the Discussion.

Calcification rates of various skeletal parts. Table 3 shows the calcification rates of the different skeletal parts of six medium-sized *Tripneustes gratilla elatensis*. Whole-test calcification rates were calculated from the sum of the various components' rates, multiplied by their weight fraction. On average, it was $1.32 \pm 0.27\%\ d^{-1}$.

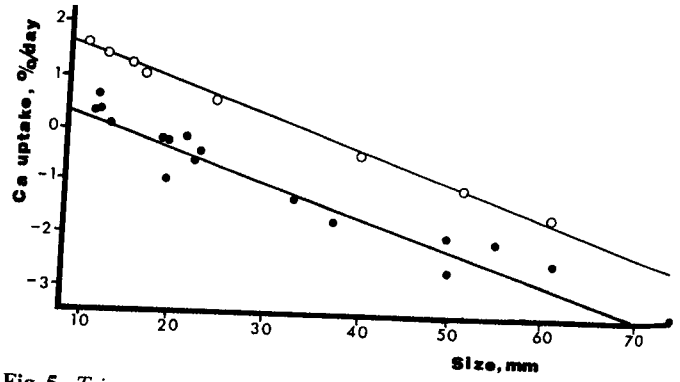

Fig. 5. *Tripneustes gratilla elatensis.* Size dependence of ^{45}Ca (●) and allometrically determined (○) calcification rates (% d^{-1}, logarithmic scale) of whole tests

Table 3. *Tripneustes gratilla elatensis.* Absolute (CA, % d^{-1}) ^{45}Ca determined calcification rates, and relative to coronal calcification (%), of different skeletal components. PW: partial weight of component, relative to total dry skeletal weight (percentage)

Urchin no.	1		2		3		4		5		6		Mean weight and calcification rates (± SD)		
Diameter, mm	19.8		25.7		26.5		29.8		31.5		34.2			Calcification	
Skeletal part	CA	%	CA	%	CA	%	CA	%	CA	%	CA	%	PW (%)	CA	%
Coronal test	1.14	100	1.67	100	1.34	100	2.28	100	1.43	100	1.22	100	65±6	1.514±0.419	100
Whole test	1.09	95	1.54	93	1.14	85	1.75	77	1.24	87	1.17	96	100	1.322±0.266	89± 7
Apical plates	0.96	83	1.44	86	1.09	82	2.34	102	1.07	75	0.95	78	1±2	1.309±0.536	84±10
Spines	0.85	74	1.25	75	0.70	52	0.76	33	0.37	26	0.65	54	23±6	0.766±0.288	52±20
Lantern	1.12	98	1.60	96	1.02	76	1.84	80	1.41	99	1.20	99	11±1	1.368±0.310	92±10
Hypophysis	0.87	76	1.44	86	1.12	84	1.72	75	0.88	61	0.88	72	1±0	1.151±0.359	76± 9
Rotula	1.09	95	1.56	94	1.38	103	1.74	76	1.11	77	0.80	66	1±0	1.280±0.347	85±14
Half pyramid	0.72	63	1.07	64	1.05	78	1.54	67	0.94	65	0.63	52	7±0	0.992±0.321	65± 8
Teeth	1.68	147	1.84	110	2.67	200	2.69	118	2.35	164	1.51	124	2±0	2.124±0.517	143±34
Teeth, lower part		–	1.23	74	0.78	58	1.35	59	–	–	0.49	40	–	0.960±0.401	58±14
Teeth, upper part		–	7.93	476	4.95	370	7.20	315	–	–	4.52	372	–	6.150±1.673	383±67

Since the coronal test is the largest component (65% in DW), the other components' calcification rates were related to it as percentage. This enabled the comparison between relative calcification rates and allometric trends shown by the same components. Thus a more slowly calcifying skeletal component should show a negative allometry when compared to the coronal. As expected, the calcification rate of the apical plates was 1.3% d^{-1}, 84% of the coronal, in agreement with an allometric coefficient of 0.824 for apical size vs test diameter (Table 1 B). The size of regular echinoid's spine is known to have a negative allometry with diameter size (0.77 to 0.87: Regis, 1969, 1973). Although we did not measure *Tripneustes gratilla elatensis* spines, a negative allometry is suggested by the relatively low spine calcification (52% of the coronal).

The calcification rate of Aristotle's lantern (1.37% d^{-1}: 92% of the coronal) was somewhat higher than expected from allometry ($b/r=0.824$: Table 1 D). While the calcification of its sub-units, half-pyramids, hypophyses etc., 65 to 85% of the coronal, agreed with the above allometry, the teeth showed exceedingly high calcification (2.2% d^{-1}). Moreover, the proximal (upper) part of the teeth calcified at a rate six times higher than the distal, eroding tips.

Calcification and weight gradients along the plate column. Fig. 6 shows the dry weight (DW) of IA plates as a function of their meridional position (distance from the peristome) for individuals of various sizes (D=22 to 72 mm). All, except the several primordial plates, are recruited to the plate column at the apex, gradually shifting downwards, but no plates are eliminated. Therefore the weight patterns of the various urchins reveal the ontogenetic trends: (a) All the plates increase their skeletal weight, (b) while the ambitus line, characterized by the largest plates, gradually shifts to higher plates. Fig. 6 also indicates that, although the dry weight pattern is similar for all urchins, larger urchins' curve-lines are more

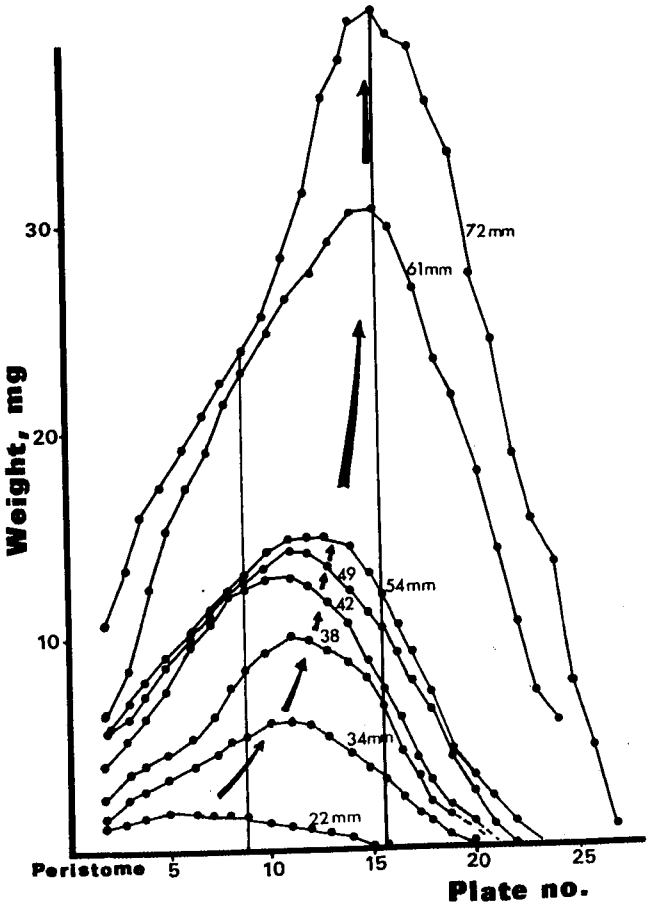

Fig. 6. *Tripneustes gratilla elatensis.* Dry skeletal weight of IA plates of eight different-sized urchins, arranged according to distance from the peristome. Vertical bars trace the growth of certain plates, Nos. 9 and 16, while arrows mark the relative upwards shift of the ambitus

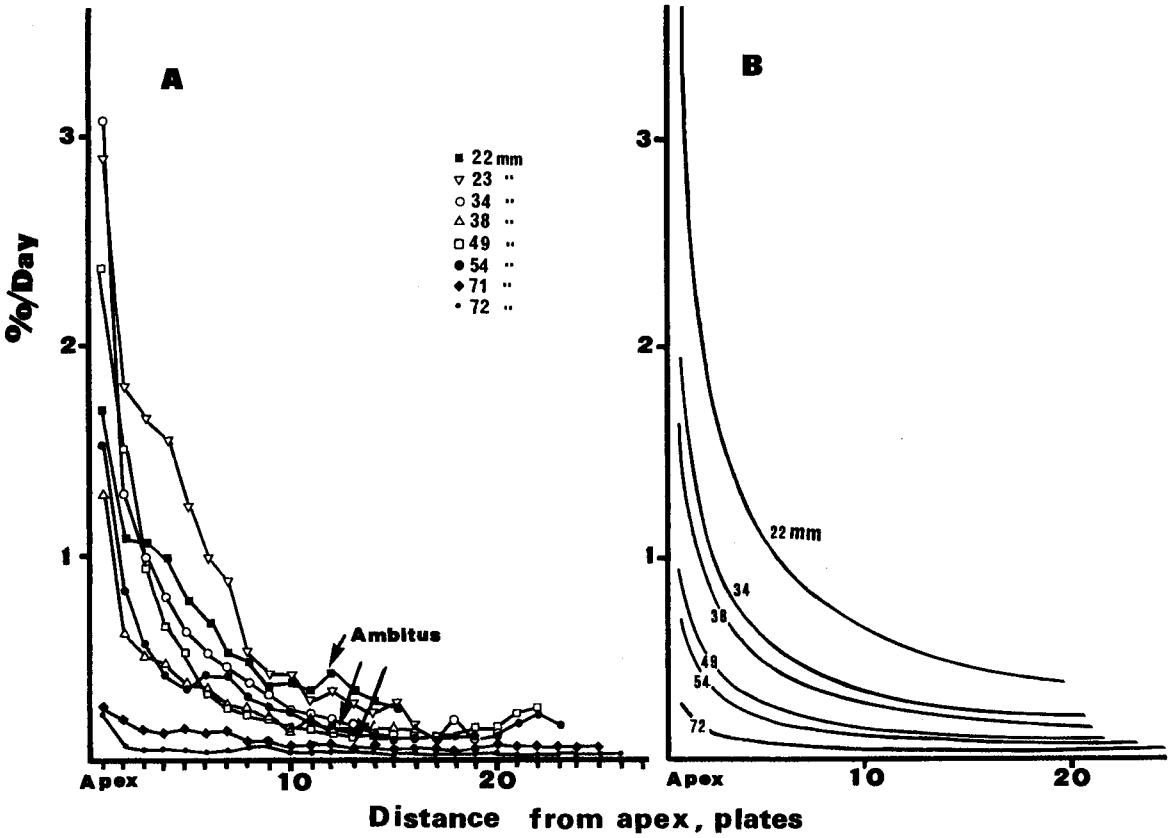

Fig. 7. *Tripneustes gratilla elatensis.* A: Per plate calcification rates (% day^{-1}) of different-sized urchins as function of their distance from the apex (in plate numbers). B: Model curves calculated from Eq. (14)

humped, suggesting that ambital plates grow faster than the terminal ones, adoral and aboral.

In spite of individual variation, the calcification patterns of these individuals showed a common trend (Fig. 7A). The plates next to the apex showed the highest calcification rates, strongly decreasing as they move away towards the peristome. Therefore, it seems logical to relate plate calcification rate (Y) to the distance from the apex (X), and a power function is suggested:

$$Y = aX^b \qquad (12)$$

$X = 1, 2, 3 \ldots N$ (plate numbers counted downward),

where a = calcification rate of the uppermost plate (X = 1); b = gradient coefficient and N = total number of plates per column. Note that in the conventional morphologic notation, used elsewhere in this paper, plate numbers are counted from the peristome upwards. After calculating the regression slope for each urchin, the regression between a and b with the urchin size D was attempted (Table 4). A fair correlation existed only between a and D:

$$a = 11.58 \exp(-0.053\ D) \quad (n = 9, r = 0.81). \qquad (13)$$

Combining Eq. (12) and Eq. (13), and using mean b value (-0.762 ± 0.238, Table 4), a corrected version of Eq. (12) emerges:

$$Y = 11.58 \exp(-0.053\ D)\ X^{(-0.762)}. \qquad (14)$$

Table 4. *Tripneustes gratilla elatensis.* Calcification rates and gradient along the interambulacral plate column of different-sized urchins [components of Eq. (13)]. The order of plates from the apex downward (see also Fig. 7). *N:* no. of plates per column

Urchin size (D, mm)	No. plates (*N*)	Maximal calc. rate (a, % d^{-1})	Gradient coefficient (b)*	Correlation coefficient (*r*)
22	16	1.755	−0.658	0.901
23	16	4.617	−1.068	0.945
34	20	3.366	−1.117	0.981
38	19	1.121	−0.693	0.965
49	21	0.251	−0.452	0.822
49	22	2.228	−0.967	0.928
54	23	1.386	−0.762	0.938
71	26	0.289	−0.525	0.927
72	27	0.147	−0.612	0.958

* Mean of this column is $b = -0.762 \pm 0.238$

Using Eq. (14) we calculated model curves for *Tripneustes gratilla elatensis* of various sizes (Fig. 7B). It is noteworthy that the gradient coefficient (−0.053) was identical to that of total calcification vs size [Eq. (9)].

Sutural calcification. Fig. 8 presents the plate-edge calcification patterns of interambulacral plates of a 49-mm individual, compared with size increment patterns of a

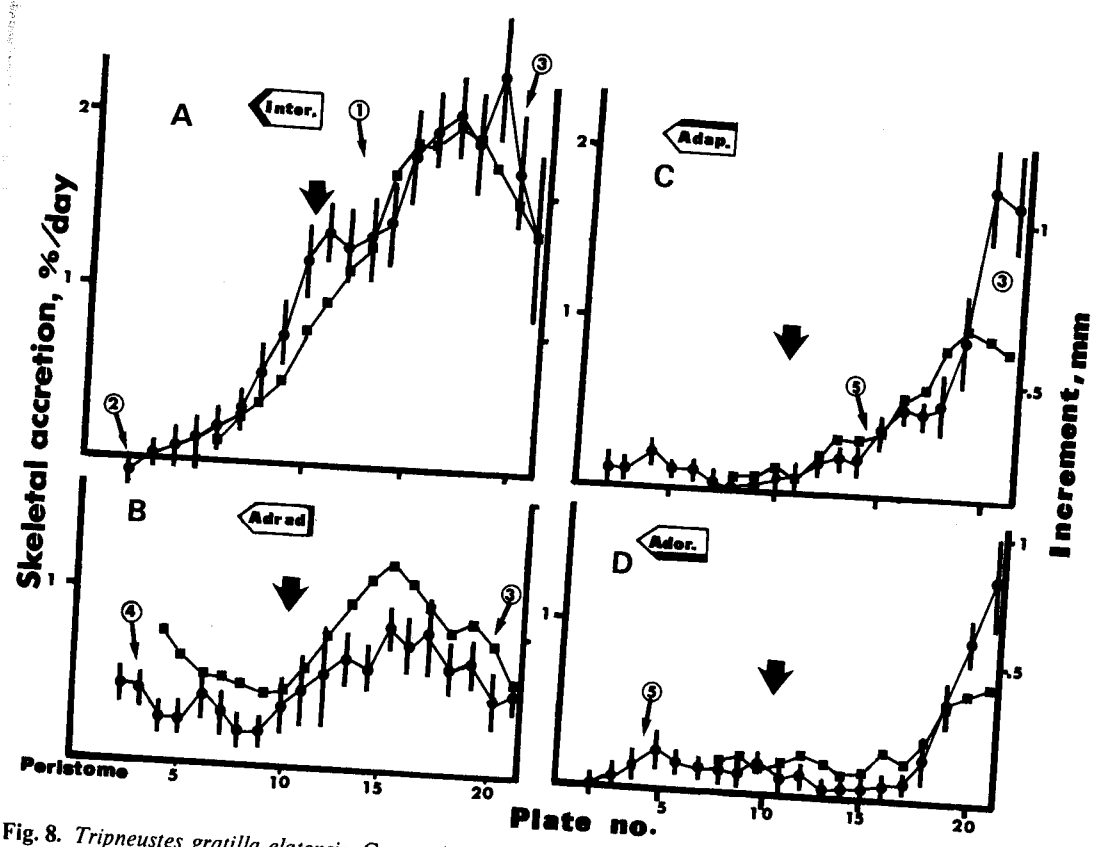

Fig. 8. *Tripneustes gratilla elatensis.* Comparison between net IA sutural calcification rates of a 49-mm individual (●), and growth-line increments (■) in IA plates of a 51-mm individual. A to D: peripheral margins (interradiad, adradiad, adapicad and adorad). Plates are counted upwards. Thick arrows point at the approximate position of the ambitus. Numbered arrows point at characteristic trends (see text)

51-mm individual, based on growth-line measurements. If one assumes that the sutural margins grow both peripherally and perpendicularly to their wide surfaces, net sutural calcification was obtained by deducting the calcification rate of the plate median (Fig. 2) from the peripheral (gross) rates. Thus, net calcification rates represent directional accretion of the plate edge, and such a comparison with measurable size increment is justified.

Both methods, the radioactive and the method based on optical measurements, agreed well with one another, displaying the following typical trends (numbered arrows in Fig. 8): (1) Along the interradial, zig-zag suture (Fig. 8A), the highest calcification rates are shown super-ambitally, strongly decreasing in plates beneath the ambitus. (2) In the plates next to the peristome, the interradial suture calcified less than the plate median, hence the apparent negative net calcification values shown in these plates. (3) The margins of the uppermost plates, next to the apex, calcified less than the plates beneath, in most directions. (4) Adradiad calcification (towards the suture between Amb and IA plates, Fig. 8B) was usually less than the interradiad, but this situation reversed sub-ambitally, where adradiad calcification increased greatly above the interradiad. (5) In the meridional (vertical) direction (Fig. 8C and 8D), the adapicad (upper) and adorad (lower) sutural edges' rates were highest in the 2 to 3 uppermost plates. Super-ambitally, adapicad calcification usually exceeded the adorad, while sub-ambitally the adorad calcification was higher.

Fig. 9 presents the IA sutural patterns of four urchins of different size. Although the method varied slightly (only one sample was taken and the plate median was not discounted), the size dependence shows clearly. While smaller urchins shared well-defined patterns, older individuals showed more subdued patterns, with almost equal calcification rates in opposite sutures.

The sutural calcification pattern of ambulacral plates (Fig. 10) was quite different from the IA. While the super-ambital plates showed the highest rates, decreasing sub-ambitally in the meridional direction (Fig. 10A), the upwards directed (adapicad) calcification rates were consistently higher than the adorad, whereas in the horizontal direction (Fig. 10b) the perradiad suture (towards the Amb mid-suture) calcified less than the adradiad suture rates.

In all the circum-ambital plates, horizontal calcification dominated over meridional (vertical). An index, v/h ratio, which measures the vertical vs horizontal uptake of ^{45}Ca, is suggested to express this dominance. It is calculated as the calcification values of the adapicad and adorad suture margins combined, divided by the sum of the interradiad and adradiad rates. The v/h ratios of IA plates for the urchins (calcification patterns shown in Fig.9) are given in Table 5. It appears that v/h ratio of the plates at ambitus level (9 to 17, according to size) rarely exceeded

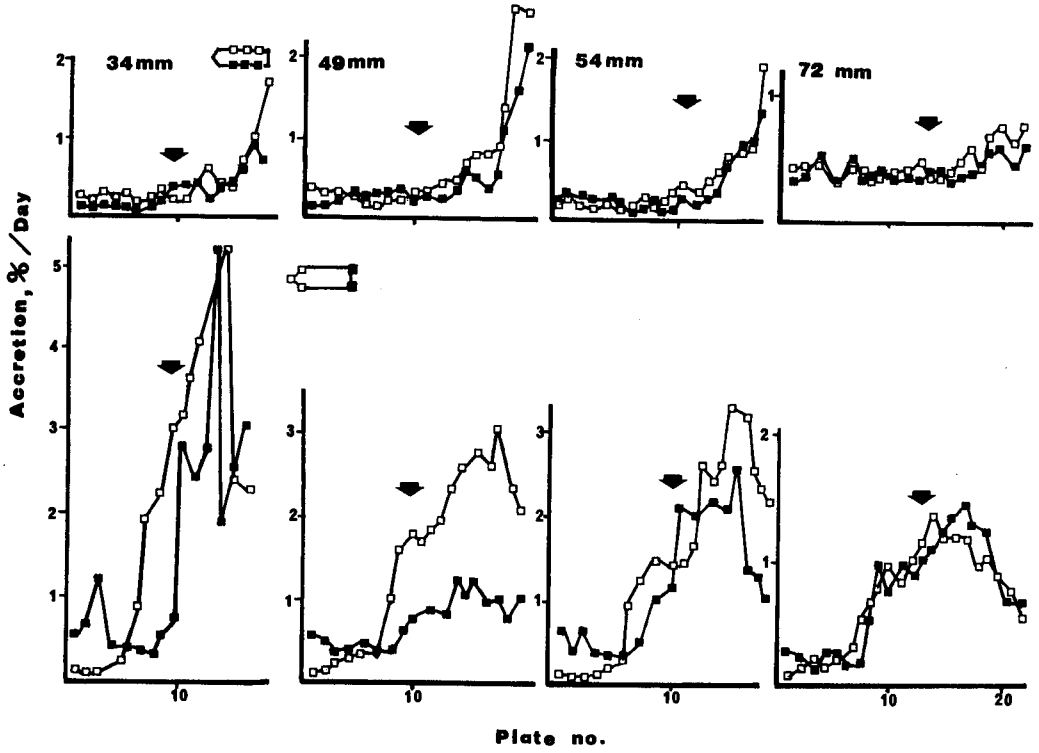

Fig. 9. *Tripneustes gratilla elatensis.* IA sutural calcification patterns of *T. g. elatensis,* with a diameter of 34, 49, 54 and 72 mm, vertically (upper) and horizontally (below)

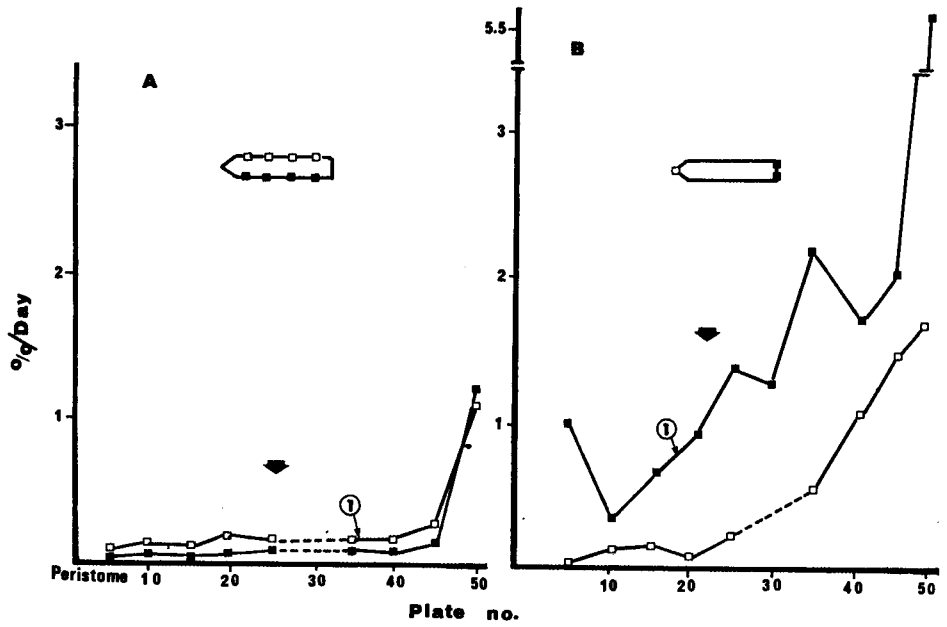

Fig. 10. *Tripneustes gratilla elatensis.* Differential ambulacral calcification pattern of a 49-mm individual; A: vertically and B: horizontally

v/h = 0.3. The uppermost plates grow rapidly in all directions, hence their excessive v/h, whereas the high v/h ratio shown by the lowermost plates is caused mainly by an equal decrease in all directions.

Discussion

The radioactive method is prone to considerable inaccuracy due to post-incubation isotopic deposition (Barnes and Crossland, 1977) and to the existence of internal Ca exchangeable pools: the first effect can be avoided by appropriate methodology, but the second poses a more fundamental problem in calcification rate assessment. Even so, this method gives significant results in short-term experiments and offers an opportunity to trace the Ca pathway through the different compartments of *Tripneustes gratilla elatensis.*

Since short-term experiments are strongly affected by these pools (Böhm and Goreau, 1973), which gave funda-

Table 5. *Tripneustes gratilla elatensis.* The ratio between vertically and horizontally directed sutural calcification rates (v/h ratio), for different-sized urchins. Plate order from peristome upward

Plate no.	Sea urchin size (mm)				Mean ± SD
	34	49	54	71	
1+2	0.50	0.60	0.31	–	0.47±0.15
3	0.38	0.44	0.94	0.32	0.52±0.28
4	0.23	1.04	0.45	0.80	0.63±0.36
5	0.52	0.88	0.39	1.14	0.73±0.34
6	0.36	0.50	0.47	–	0.44±0.07
7	0.25	0.43	0.22	0.86	0.44±0.29
8	0.18	0.25	0.18	0.56	0.29±0.18
9	0.16	0.24	0.12	0.34	0.22±0.10
10	0.06	0.25	0.12	0.12	0.14±0.08
11	0.05	0.17	0.13	0.15	0.13±0.05
12	0.06	0.22	0.15	0.16	0.15±0.07
13	0.09	0.17	0.14	0.24	0.16±0.06
14	0.06	0.18	0.21	0.18	0.16±0.07
15	0.06	0.19	0.11	0.13	0.12±0.05
16	0.06	0.27	0.18	0.11	0.15±0.09
17	0.36	0.24	0.17	0.19	0.24±0.09
18	0.43	0.36	0.18	0.21	0.30±0.12
19	–	0.56	0.35	0.13	0.35±0.20
20	–	1.27	0.38	0.43	0.69±0.50
21	–	1.52	0.88	0.50	0.97±0.51

mentally different exchange kinetics from the calcification process itself (Böhm, 1978; Borowitzka, 1979), the discrepancy between short- and long-term experiments may be caused by these pools. The existence of the pools is suggested by the higher calcification rates obtained under longer ^{45}Ca exposures, or when NRSW post-incubation was used. They apparently store ^{45}Ca during earlier exposure, releasing it during late exposure and in post-incubation. Under optimal conditions, with these pools fully saturated, the ^{45}Ca incorporation rates will approach the calcification rates obtained by morphmetric methods. Hence, the F-ratio between estimates based on radioactive and allometric calcification, increasing with exposure length and in urchins which had longer post-incubation, is also related to these pools.

Being the largest organic component, the coelomic fluid is the most likely tissue in which Ca may be stored for prolonged time periods. An estimate of the storage capacity of this pool can be obtained from the F-ratio, or rather from the difference between high and low F values under the different conditions. The highest calcification rate of a 13-mm urchin, with a skeletal weight of 120 mg (calculated from Table 1F), was 2.8% d^{-1} (=3.3 mg $CaCO_3$). The volume of the coelomic cavity, 30% of the body wet weight of 870 mg (=800 μl), is ca 250 μl. Hence, the absolute Ca uptake is 33 μmol Ca (or 3.3 mg $CaCO_3$). As indicated by the F-differences, about 30% of this quantity (10 μmol) is retained in the coelom for later deposition, and the Ca concentration is 40 mmol l^{-1} (10 μmol/250 μl). Thus, the coelomic Ca pool concentration estimate is three times higher than the normal seawater Ca concentration (12 mmol l^{-1}).

These estimates agree well with the relatively high coelomic Ca uptake rates and Ca concentrations found by Kaneko *et al.* (1981b, 1982). On the other hand, the indirect measurements of skeletal weight and use of field data to obtain weight of laboratory urchins may have caused overestimation of F-ratios and pool size. It is obvious that the short incubations (6 to 24 h) did not saturate the pools. The F-ratio decrease with size [Eq. (11)] implies that the saturation of the pools of larger urchins may be a slower process.

Although advantageous from the viewpoint of pool saturation, longer exposures in closed systems are less desirable. Depletion of the ion and accumulation of waste material may impair the balance between organic growth and calcification, resulting in fragile, poorly-calcified tests (Dafni and Erez, 1987). Therefore, the assumption of a uniform calcification rate during such long exposures may lead to erroneous results.

Although it is less accurate for estimating absolute growth rates, the radioactive method is fairly accurate in obtaining relative rates. A demonstration of its high resolution power is the close agreement between relative calcification rates of various skeletal components (Table 3) and their allometry (Table 1), and the fit between allometric and radioactive measurements of plate-edge growth (Fig. 8). The apparent exception, a relatively rapid calcification shown by the lantern, higher than predicted by allometry, is explained by the faster growth of the teeth and the constant wearing-out of their tips. ^{45}Ca specific activity of the teeth increases both by the intensive ^{45}Ca deposition at the growing upper end, and by the erosion of non-radioactive Ca in the lower part. Here, contrary to other skeletal components, the relative calcification rates of teeth depend on exposure length. Kaneko *et al.*'s (1981b) record of high ^{45}Ca incorporation rates in echinoid teeth (18 times higher than the coronal), is thus easily explained by the long radioactive exposure (28 d).

Whole-plate weight and calcification curves (Figs. 6, 7) reflect the ontogeny of the individual plates. The symmetrical plate-weight patterns (Fig. 6) may suggest that there is a symmetry in growth or calcification in both sides of the ambitus. Yet, calcification rate patterns (Fig. 7) demonstrate a sharp decrease in calcification (per g skeleton) occurring when the plates move away from the apex. Consequently, a plate grows fast initially, slowing down as it moves towards the ambitus. Beneath the ambitus level, the plate size almost does not change, but younger and still larger plates accumulate on top of it, causing the ambital diameter to expand. Thus, by calcifying in rates and patterns suiting their vertical position, the plates maintain the typical size relations, without having to resorb skeletal matter.

The curve shown in Fig. 7 is somewhat similar to the parabolic curve offered by Raup (1968) to describe the same gradient for another echinoid species, *Strongylocentrotus pallidus,* predicting strong decrease from the apex downwards, and an increase while the plates approach the peristome. However, the slight increase shown in the

lowermost plates of some individuals (Fig. 7 A), obviously due to secondary deposition at the peristome edge, scarcely affects the general pattern.

Porosity is also a good measure of growth. Faster-growing plates are highly porous, since most of the skeleton is invested in peripheral accretion, while periods of non-growth are characterized by deposition inside the stereom mesh, resulting in reduced porosity. Older urchins and individuals maintained in the laboratory for longer periods, consequent to deformation, grew slowly and had compact tests (Dafni and Erez, 1987). The high porosity of the lowermost plates is explained by their increased thickness, with the deposition of the perignathic girdle bordering the peristome rim.

In spite of minor differences, the plate-edge patterns derived from the radioactive and the allometric measurements (Fig. 8) were almost identical. The rather complex patterns, subject to strong variation in individuals of different size, were strikingly similar to plate-edge patterns that Märkel (1975, 1976) found for two Mediterranean echinoids by the method of tetracyclin-induced growth-lines.

Tallness is a most prominent feature in regular echinoid morphology. Although it is basically species-specific, it may also differ in different habitats (McPherson, 1965; Fuji, 1967; Ernst, 1973), or changes due to pollution (Dafni, 1980, 1983 b). It is related to the ratio between the vertical and horizontal calcification of the plate edges (v/h) (Table 5). Firstly, it reflects the tendency of skeletal plates to grow mainly horizontally, so that together with the continuous insertion of new plates apically, the almost unchanged test profile is accounted for (expressed in its height vs diameter ratio: H/D). Secondly, abnormally high v/h ratios may foretell future changes in tallness (H/D ratio), as in the case of skeletal deformations (Dafni, 1980, 1983 a, b; Dafni and Erez, 1987).

We propose recognizing the v/h ratio of circumambital IA plates as an index of morphogenetic determination in regular echinoids. It can be applied in short-term ^{45}Ca assays to study the effect of various experimental and environmental conditions on the sutural calcification, and consequently on the entire echinoid test morphology.

One may conclude that the application of the radiotracer method to echinoid growth rate measurements is the first necessary step towards modelling the various growth patterns, thus revealing the regulation mechanisms that may determine their morphogenesis. A hypothetic model, based on observations and morphometric evidence, has recently been proposed to explain echinoid growth and morphogenesis in terms of "stress-balance" (Dafni and Erez, 1982; Dafni, 1985, 1986). According to this model, the sutural calcification pattern of echinoid plates is controlled by an internal mechanical array of forces, among which are increased volume of the coelomic fluid, and the effect of contractile and elastic tissue elements. Tensional forces across the sutures apparently pull apart the plates, thus inducing growth, while compression causes growth cessation.

Acknowledgements. We would like to thank Professor F. D. Por for his advice throughout the study. The H. Steinitz Marine Laboratory staff, in particular Drs. A. Baranes and A. Diamant, offered help and encouragement. Professor L. Fishelson and Dr. J. Kendall read early drafts of the manuscript and their comments are appreciated.

Literature cited

Barnes, D. J. and C. J. Crossland: Coral calcification: sources of error in radioisotope technique. Mar. Biol. *42*, 119–129 (1977)

Barnes, D. J. and C. J. Crossland: Variability in the calcification rate of *Acropora acuminata* measured with radioisotopes. Coral Reefs *1*, 53–75 (1982)

Böhm, L.: Application of the ^{45}Ca tracer method for determination of calcification rates in calcareous algae: effect of calcium exchange and differential saturation of algal calcium pools. Mar. Biol. *47*, 9–14 (1978)

Böhm, L. and T. F. Goreau: Rates of turnover and net accretion of calcium and role of calcium binding polysaccharides during calcification in the calcareous alga *Halimeda opuntia* (L.). Int. Revue ges. Hydrobiol. *58*, 723–740 (1973)

Borowitzka, M. A.: Calcium exchange and measurement of calcification rates in the calcareous red alga *Amphiroa foliacea*. Mar. Biol. *50*, 339–347 (1979)

Chamberlain, J. A. Jr.: Mechanical properties of coral skeleton, compressive strength and its adaptive significance. Paleobiology *4*, 419–435 (1978)

Dafni, J.: Abnormal growth patterns in the sea urchin *Tripneustes* cf. *gratilla* (L.) under pollution (Echinodermata: Echinoidea). J. exp. mar. Biol. Ecol. *47*, 259–279 (1980)

Dafni J.: A new subspecies of *Tripneustes gratilla* from the northern Red Sea (Echinodermata: Echinoidea: Toxopneustidae). Isr. J. Zool. *32*, 1–12 (1983 a)

Dafni, J.: Aboral depressions in the tests of the sea urchin *Tripneustes* cf. *gratilla* (L.) in the Gulf of Eilat, Red Sea. J. exp. mar. Biol. Ecol. *67*, 1–15 (1983 b)

Dafni, J.: Skeletal growth and calcification in the short-spined sea urchin (*Tripneustes gratilla elatensis*). Ph.D. dissertation 109+V pp., Hebrew University of Jerusalem. Hebrew with English summary 1984

Dafni, J.: Effect of mechanical stress on the calcification pattern in regular echinoid skeletal plates, pp 233–236. *In:* Echinodermata. Proc. 5th int. Echinoderm Conf., Galway, Sept. 1984. Ed. by B. F. Keegan and B. D. S. O'Connor. Rotterdam: Balkema 1985

Dafni, J.: A biomechanical model for the morphogenesis of regular echinoid tests. Paleobiology *12*, 143–160 (1986)

Dafni, J. and J. Erez,: Differential growth in *Tripneustes gratilla* (Echinoidea), pp 71–75 *In*: Echinoderms. Proc. 4th int. Echinoderm Conf., Tampa Bay. Ed. by J. M. Lawrence. Rotterdam: A. A. Balkema 1982

Dafni, J. and J. Erez: Skeletal calcification patterns in the sea urchin *Tripneustes gratilla elatensis* II. Effect of various treatments. Mar. Biol. *95*, 289–297 (1987)

Deutler, F.: Über das Wachstum des Seeigelskeletts. Zool. Jb. (Anat.) *48*, 119–200 (1926)

Ebert, T. A.: Growth rates of the sea urchin *Strongylocentrotus purpuratus* related to food availability and spine abrasion. Ecology *49*, 1075–1091 (1968)

Ebert, T. A.: Longevity, life history, and relative body wall size in sea urchins. Ecol. Monogr. *52*, 353–394 (1982)

Ernst, G.: Actuopaläontologie und Merkmalsvariabilität bei Mediterranen Echiniden und Rückschlüsse auf die Ökologie und Artumgrenzung fossiler Formen. Paläontol. Z. *47*, 188–216 (1973)

Goreau, T. F.: The physiology of skeletal formation in corals. I. A method for measuring the rate of calcium deposition by corals under different conditions. Biol. Bull. mar. biol. Lab., Woods Hole *116*, 59–75 (1959)

Gould, S. J.: Allometry and size in ontogeny and phylogeny. Biol. Rev. *41*, 587–640 (1966)

Heatfield, B. M.: Calcification in echinoderms: effect of temperature and Diamox on incorporation of ^{45}Ca *in vitro* by regenerating spines of *Strongylocentrotus purpuratus* Biol. Bull. mar. biol. Lab., Woods Hole *139*, 151–163 (1970)

Huxley, J. S.: Problems of relative growth. New York: Dial Press 1932

Jensen, M.: The ultrastructure of the echinoid skeleton. Sarsia *48*, 39–48 (1972)

Johnson, N. O.: A trend line for growth series. J. Am. Stat. Ass. *30*, 717 (1935)

Fuji, A.: Ecological studies on the growth and food consumption of Japanese common littoral sea urchin, *Strongylocentrotus intermedius* (A. Agassiz). Mem. Fac. Fish., Hokkaido Univ. *15*, 83–160 (1967)

Kaneko, I., Y. Ikeda and H. Ozaki: Absorption of calcium through digestive tract in the sea urchin. Bull. Jap. Sci. Fish. *47*, 1421–1424 (1981 a)

Kaneko, I., Y. Ikeda and H. Ozaki: Absorption of calcium from sea water and its excretion in sea urchin. Bull. Jap. Sci. Fish. *47*, 1425–1430 (1981 b)

Kaneko, I., Y. Ikeda and H. Ozaki: Calcium level of each part in sea urchin. Bull. Jap. Sci. Fish. *48*, 11–13 (1982)

Krumgaltz, B. S.: Calcium distribution in the world ocean waters. Oceanologia Acta *5*, 121–128 (1982)

Märkel, K.: Wachstum des Coronarskeletes von *Paracentrotus lividus* Lmk. (Echinodermata: Echinoidea). Zoomorphologie *82*, 259–280 (1975)

Märkel, K.: Struktur und Wachstum des Coronarskeletes von *Arbacia lixula* Linné (Echinodermata: Echinoidea). Zoomorphologie *84*, 279–299 (1976)

Märkel, K.: Experimental morphology of coronar growth in regular echinoids. Zoomorphology *97*, 31–52 (1981)

McPherson, B. F.: Contributions to the biology of the sea urchin *Tripneustes ventricosus*. Bull. mar. Sci. *15*, 228–244 (1965)

Moss, M. L. and M. M. Meehan: Sutural connective tissues in the test of an echinoid *Arbacia punctulata*. Acta Anat. *66*, 279–304 (1967)

Moss, M. L. and M. M. Meehan: Growth of the echinoid test. Acta Anat. *69*, 409–444 (1968)

Nauen, C. E. and L. Böhm: Skeletal growth in the echinoderm *Asterias rubens* L., estimated by ^{45}Ca labelling. J. exp mar. Biol. Ecol. *38*, 261–269 (1969)

Pearse J. S. and V. B. Pearse: Growth zones in the echinoid skeleton. Am. Zool. *15*, 731–753 (1975)

Raup, D. M.: The endoskeleton. *In*: Pysiology of Echinodermata, pp 379–395. Ed. by R. A. Boolootian. New York: Interscience 1966

Raup, D. M.: Theoretical morphology of echinoid growth. J. Paleontol. *42* (Suppl.), 50–63 (1968)

Regis, M. B.: Premières données sur la croissance de *Paracentrotus lividus* Lmk. Téthys *1*, 1049–1056 (1969)

Regis, M. B.: Premières données sur la croissance de l'echinid *Arbacia lixula* (L.). Téthys *5*, 167–172 (1973)

Ricker, W. E.: Linear regression in fishery research. J. Fish. Res. Bd Can. *30*, 409–434 (1973)

Smith, A. B.: Stereom microstructure of the echinoid test. Spec. Pap. Palaeont. *25*, 1–81 (1980)

Strathmann, R. R.: The role of spines in preventing structural damage to the echinoid test. Paleobiology *7*, 400–406 (1981)

Telford, M.: Domes, arches and urchins: the skeletal architecture of echinoids (Echinodermata). Zoomorphology *105*, 114–124 (1985)

Vadas, R. L.: Preferential feeding: an optimization strategy in sea urchins. Ecol. Monogr. *47*, 337–371 (1977)

Weber, J. N.: The incorporation of magnesium into the skeletal calcites of echinoderms. Am. J. Sci. *267*, 537–566 (1969)

Weber, J., R. Greer, B. Voight, E. White and R. Roy: Unusual strength properties of echinoderm calcite related to structure. Ultrastr. Res. *26*, 355–366 (1969)

White, M., B. F. Keegan and Y. Leahy: Growth retardation in the regular echinoid *Echinus esculentus* Linnaeus. Echinodermata, pp 369–375. Proc. 5th int. Echinoderm Conf., Galway, Sept. 1984. Ed. by B. F. Keegan and B. D. S. O'Connor. Rotterdam: Balkema. 1985

Wilbur, K. M. and L. H. Jodrey: Studies on the shell formation V: the inhibition of shell formation by carbonic anhydrase inhibitors. Biol. Bull. mar. biol. Lab., Woods Hole *108*, 359–365 (1955)

Date of final manuscript acceptance: January 19, 1987.
Communicated by O. Kinne, Oldendorf/Luhe